

N O T I C E

THIS DOCUMENT HAS BEEN REPRODUCED FROM
MICROFICHE. ALTHOUGH IT IS RECOGNIZED THAT
CERTAIN PORTIONS ARE ILLEGIBLE, IT IS BEING RELEASED
IN THE INTEREST OF MAKING AVAILABLE AS MUCH
INFORMATION AS POSSIBLE

25

APR 17 1962
REC-100
MAIL ROOM
APR 17 1962

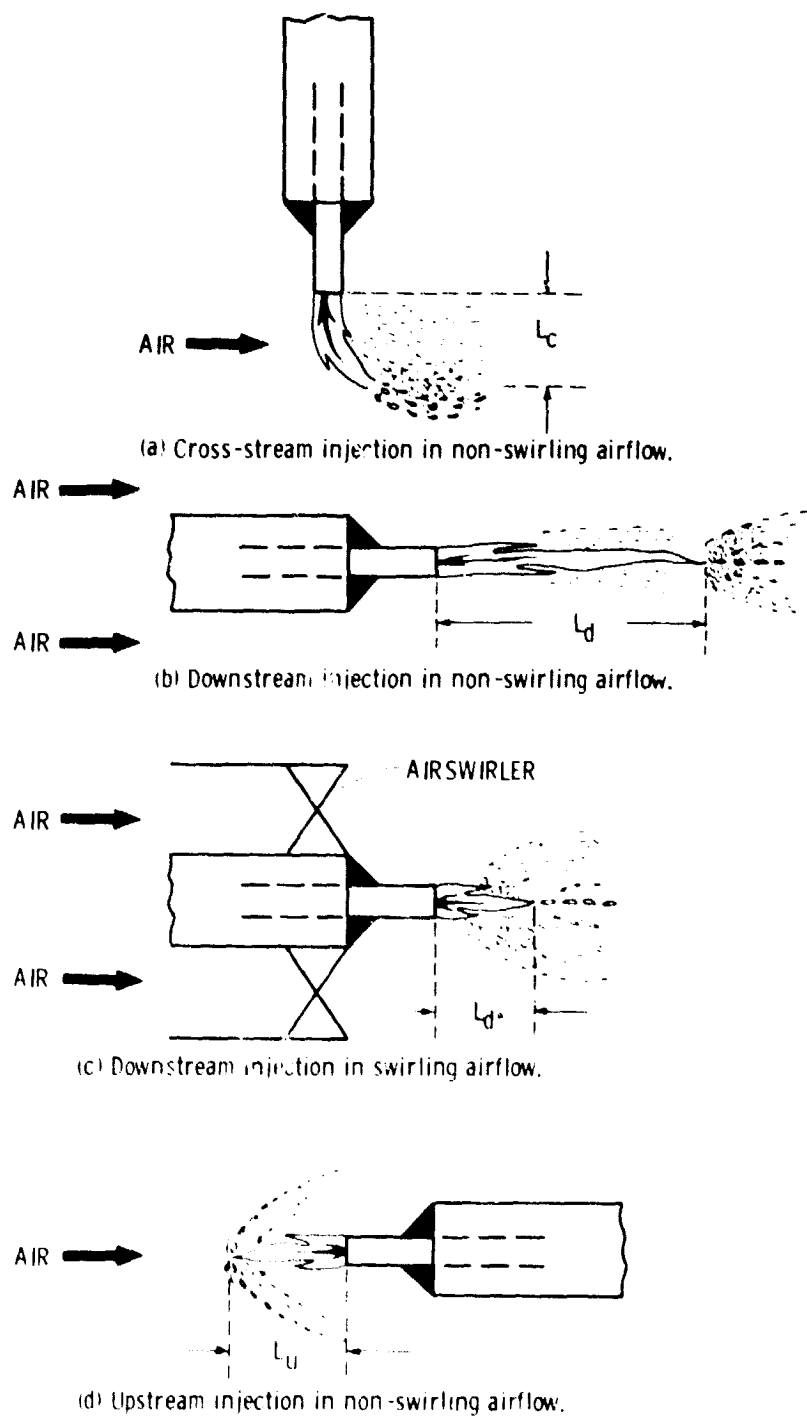


Figure 6. - Observed representations of liquid jet breakup lengths with four different injection techniques at constant relative velocity, V_r .

exhausted into the atmosphere. Airflow rate was determined with an orifice as the airflow control valve was opened until the desired airflow rate per unit area was obtained over the range of 4.6 to 25.2 g/cm²-sec. and an air velocity range of 61 to 214 m/sec. The brimouth test section shown in figure 1 has a total length of 15.2 cm, an inside diameter (of the circular duct) of 7.6 cm and it is mounted inside of a duct that is 5 m in length with an inside-diameter of 15.2 cm.

Water jets, at 293 K as determined with an I.C. thermocouple, were axially injected in the airstream by gradually opening a water flow control valve until the desired water flow rate of 68 liters/hour was obtained as measured with a turbine flowmeter. This gave liquid jet velocities of 70, 23, and 5 m/sec. for the three different injector tubes having inside diameters of 0.58, 0.102, and 0.216 cm, respectively. The tubes were 2.5 cm in length and each was inserted and centered 1.3 cm inside of a 0.64 cm outside-diameter tube and silver soldered to that tube. In tests using swirling airflow, the air swirler was mounted on the injector tube as shown in figure 2.

When the air and water flow rates were set, mean drop diameter data were obtained with the scanning radiometer mounted 11.4 cm. downstream of the open-duct exit. The scanning radiometer optical system shown in figure 3 consisted of a 1-milliwatt helium-neon laser, a 0.003-cm.-diam. aperture, a 7.5-cm.-diam collimating lens, a 10-cm.-diam converging lens, a 5-cm.-diam collecting lens, a scanning disk with a 0.05- by 0.05-cm slit, a timing light, and a photo-multiplier detector. A more complete description of the scanning radiometer, the mean drop diameter range, and the method of determining mean particle diameter are discussed in references 5 and 6.

EXPERIMENTAL RESULTS

Aerodynamic forces of conventional non-swirling and swirling airflows were utilized to breakup water jets and simulate fuel atomization in aircraft gas turbine combustors with the test facility and auxiliary equipment shown in figure 1. Mean drop diameters were determined for sprays which were produced by the three following techniques: (1) downstream injection in non-swirling airflow, (2) downstream injection in swirling airflows, and (3) upstream injection in non-swirling airflows.

Downstream Injection in Non-Swirling Airflow

Mean drop diameter data for sprays produced by three different injector tubes were obtained with the scanning radiometer for downstream injection in non-swirling airflows. The effect of mass velocity, $\rho_a V_r$, (or G) on the reciprocal mean drop diameter, D_m^{-1} , is useful in characterizing a spray in terms of surface area per unit volume of spray and may be defined as $D_m^{-1} \sim \Sigma n D^2 / \Sigma n D^3$, since it represents the reciprocal diameter of a single drop having the same area to volume ratio as that of the entire spray of droplets. At the same values of G or $\rho_a V_r$, the injector with the smallest inside diameter, 0.0584 cm, produced the largest area-to-volume ratio, D_m^{-1} . Thus, as shown in figure 4, increasing the mass velocity, $\rho_a V_r$, from 4.6 to 25 g/cm²-sec increased the spray area per unit volume as given by the following empirical relation; $D_m^{-1} \sim (\rho_a V_r)^{1.2}$.

In a previous study of the mean drop size of sprays produced by cross stream injection of liquid jets in high velocity airstreams, reference 1, it was found that the ratio of the inside diameter, D_0 , to the mean drop diameter, D_m , could be correlated with the product of the Weber number, We , and the Reynolds

number, Re , as follows; $D_0/D_m = 0.027 (WeRe)^{0.4}$ which was derived for the acceleration wave breakup regime as defined by $WeRe > 10^6$. Thus, values of D_0/D_m are plotted against values of $WeRe$ as shown in figure 5. Data for the three injector tubes are correlated with the empirical relation $D_0/D_m = 0.023 (WeRe)^{0.4}$, which is valid for the acceleration wave breakup regime since $WeRe > 10^6$.

The proportionality constant ($C_d = 0.023$) is approximately 15 percent lower than that determine for cross-stream injection ($C_c = 0.027$). The lower value of C_d was attributed to an increase in the liquid jet breakup length, L . Although it was not measured, L was assumed to vary inversely with the proportionality constant C , and observed representations of L for four different injection techniques are shown in figure 6. A comparison of figures 6(a) and (b) shows that $L_d > L_c$ which agrees with the result $C_d < C_c$. Also, with downstream injection, the aerodynamic force is exerted along the length of the jet instead of circumferentially as in the case of cross-stream injection. Thus, more time is allowed for liquid surface waves to grow in amplitude and D_m^{-1} is correspondingly decreased.

Downstream Injection in Swirling Airflow

Acceleration wave breakup data were obtained for downstream injection with a 70° blade angle axial air-swirler mounted on the injector tube as shown in figure 2. The reciprocal mean drop diameter plotted against mass velocity, as shown in figure 7, gives the relationship, $D_m^{-1} \sim (\rho_a V_r)^{1.2}$ for the three different injector tubes. The relationship is the same as that obtained with axial downstream injection in non-swirling airflow. To determine the relationship of D_m^{-1} to the product of the Weber and Reynolds numbers, the data are plotted as show in figure 8 and fall close to the empirical expression, $D_0/D_m = 0.027 (WeRe)^{0.4}$, which was obtained for cross-stream injection. Thus, $C_d^* = C_c$ and as shown in figure 6, $L_d^* = L_c$.

The shorter liquid jet breakup length, L_d^* , obtained with swirling airflow as compared with L_d for non-swirling airflow was attributed to the high degree of turbulent mixing produced by the airswirler which tended to shorten the liquid jet breakup length and thus produce smaller droplets in the spray. Also, due to airflow blockage of the airswirler, the relative velocity V_r was approximately 30 percent higher with the airswirler than without it for the same airstream approach velocity. However, at the same value of V_r , swirling airflow increased the value of the proportionality constant 15 percent above that obtained with non-swirling airflow.

Upstream Injection in Non-Swirling Airflows

When a liquid jet is injected upstream in non-swirling airflows, it is atomized and then the spray is blown back downstream so that some of the droplets are unavoidably collected on the injector surface. The collected liquid will then be re-atomized and produced a bimodal distribution of drop size that may appreciably affect the mean drop diameter measured for the total spray. With this in mind, mean drop diameters were determined and defined as D_m^* for upstream injection in non-swirling airflows. As shown in figure 9, values of mean drop diameter D_m^* are plotted against mass velocity for the two injectors and give the following linear relationship $D_m^* \sim (\rho_a V_r)^{1.5}$. Thus, in the case of upstream injection the effect of mass velocity on reciprocal mean drop diameter is somewhat greater than in the case of downstream injection. This effect on the upstream injection breakup length L_u is shown

in figure 6(c) by comparing it with L_d shown in figure 6(a).

In figure 10, the plot of D_0/D_m against $WeRe$ gives the empirical expression $D_0/D_m = 0.0045 (WeRe)^{0.5}$. Figure 10 also shows that values of D_0/D_m were not greatly different from those determined for cross stream injection in non-swirling airflows. This small difference could be caused by secondary atomization of the liquid and indicates the need of minimizing the frontal area of fuel injectors designed for upstream injection.

SUMMARY OF RESULTS

Injector performance was improved for downstream injection as characterized by a 15 percent reduction of mean drop diameter when swirling instead of non-swirling airflow was used at the same airflow rate per unit area. This was attributed to a reduction in the liquid-jet breakup length due to the high degree of turbulent mixing encountered in a swirling airflow as compared with that of non-swirling airflow and normal pipe turbulence. The correlations derived in this investigation of acceleration wave breakup of water jets, as defined by values of $WeRe > 10^6$, were as follows:

1. Downstream injection in non-swirling airflows gave the empirical relationship,
 $D_0/D_m = 0.023 (WeRe)^{0.4}$.
2. Downstream injection in swirling airflows gave the empirical relationship,
 $D_0/D_m = 0.027 (WeRe)^{0.4}$.

3. Upstream injection in non-swirling airflows gave the empirical relationship,
 $D_0/D_m = 0.0045 (WeRe)^{0.5}$.

REFERENCES

1. Ingebo, R. D., "Capillary and Acceleration Wave Breakup of Liquid Jets in Axial-Flow Air-streams," NASA TP-1791, 1981.
2. Ingebo, R. D., "Atomizing Characteristics of Swirl Can Combustor Modules with Swirl Blast Fuel Injectors," NASA TM-79297, 1980.
3. Mayer, E., "Capillary Mechanisms of Liquid Atomization in High Velocity Gas Streams," 12th International Astronautical Congress, Academic Press, New York, 1963, pp. 731-740.
4. Adelberg, M., "Mean Drop Size Resulting from the Injection of a Liquid Jet into a High-Speed Gas Stream," AIAA Journal Vol. 6, No. 6, June 1968, pp. 1143-1147.
5. Buchele, D. R., "Scanning Radiometer for Measurement of Forward-Scattered Light to Determine the Mean Diameter of Spray Particles," NASA TM X-3454, 1976.
6. Ingebo, R. D., "Effect of Airstream Velocity on Mean Drop Diameters of Water Sprays Produced by Pressure and Air Atomizing Nozzles," NASA TM-73740, 1977.

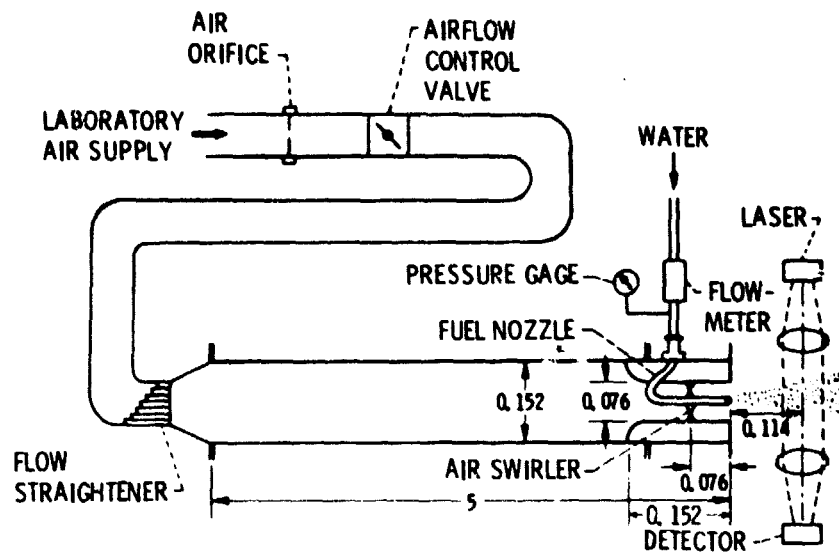


Figure 1. - Test facility and auxiliary equipment. (Dimensions are in meters.)

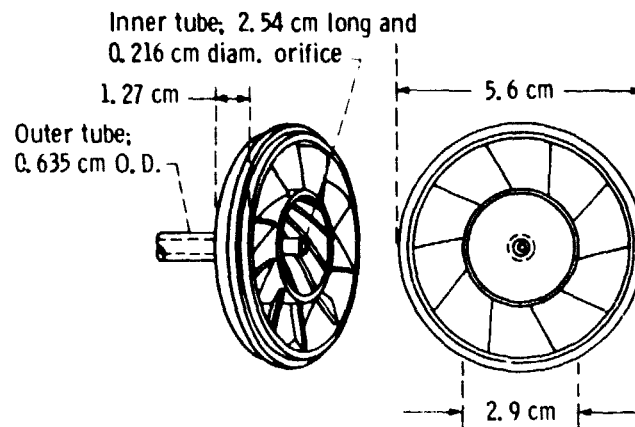


Figure 2. - 70° axial swirler (open area of 15.5 cm²) mounted on 0.635 cm O.D. tube.

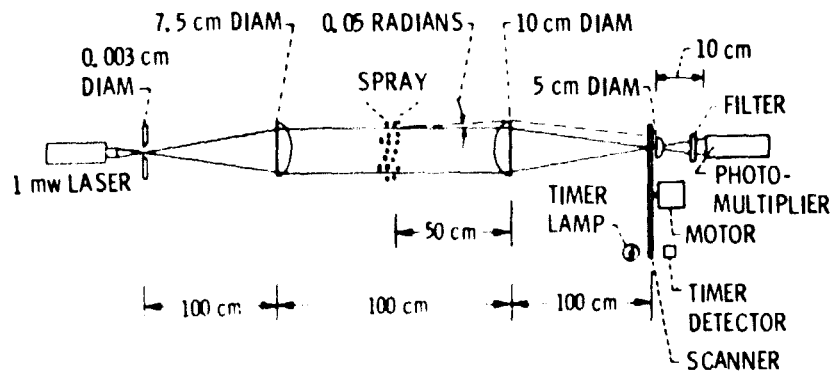


Figure 3. - Scanning radiometer optical path.

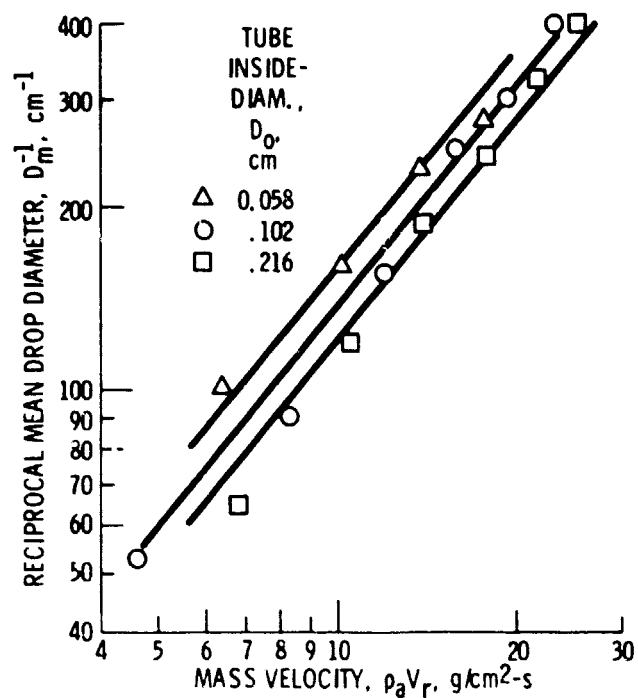


Figure 4. - Variation of reciprocal mean drop diameter with mass velocity. Axial downstream injection in axial airflow.

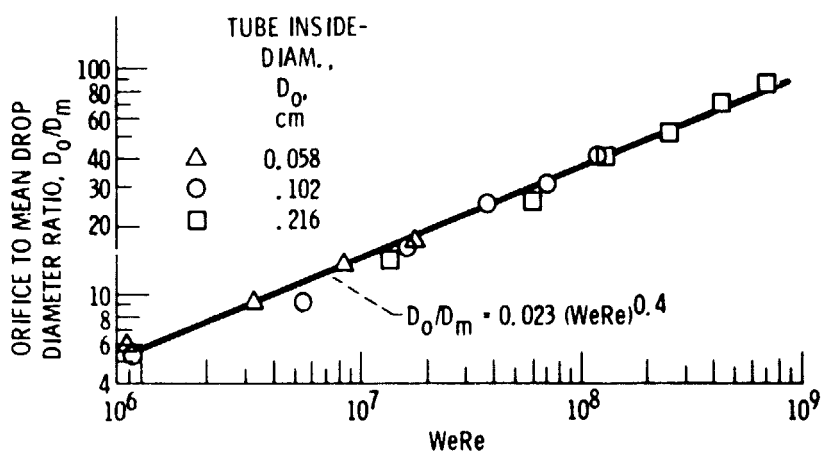


Figure 5. - Variation of orifice to mean drop diameter ratio with product of the Weber and Reynolds number. Axial downstream injection in axial airflow.

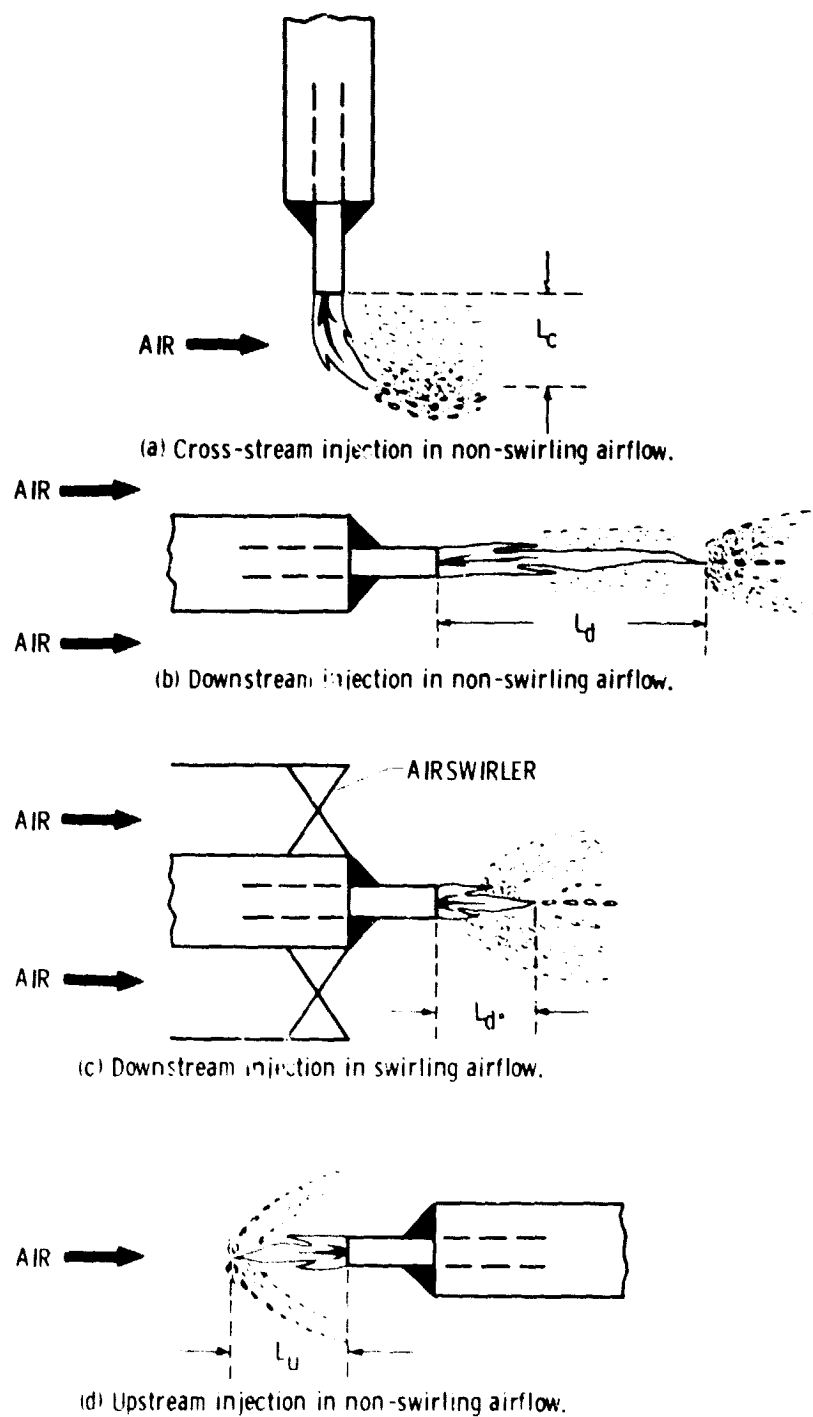


Figure 6. - Observed representations of liquid jet breakup lengths with four different injection techniques at constant relative velocity, V_r .

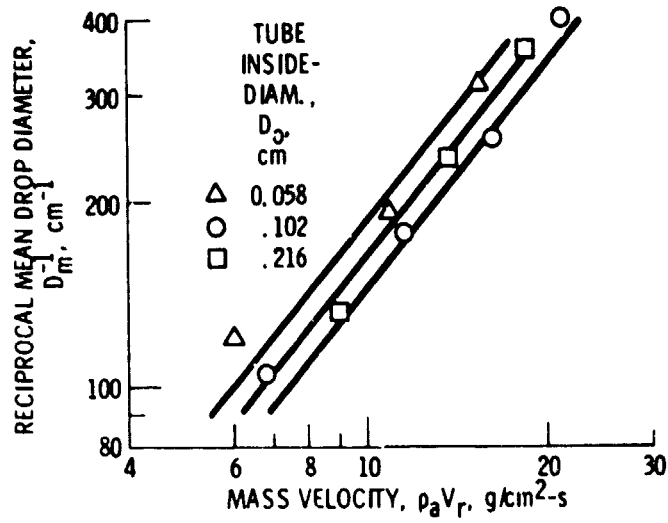


Figure 7. - Variation of reciprocal mean drop diameter with mass velocity. Axial downstream injection in swirling airflow with the 70° blade-angle air swirler.

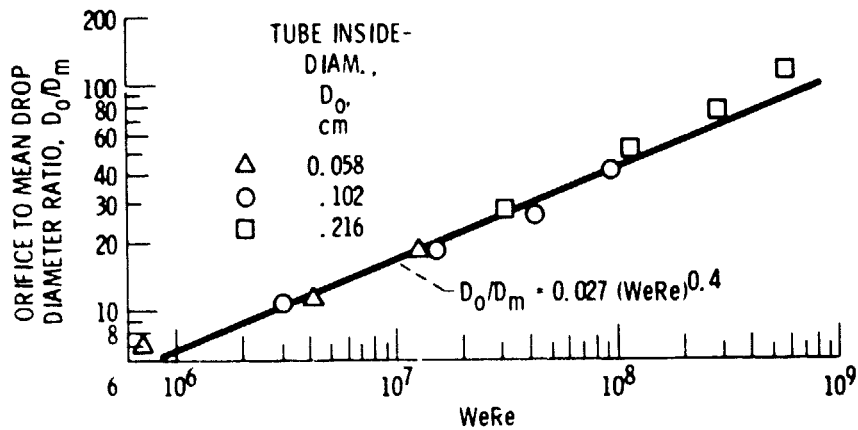


Figure 8. - Variation of orifice to mean drop diameter ratio with product of the Weber and Reynolds number. Axial downstream injection in swirling airflow with the 70° blade-angle swirler.

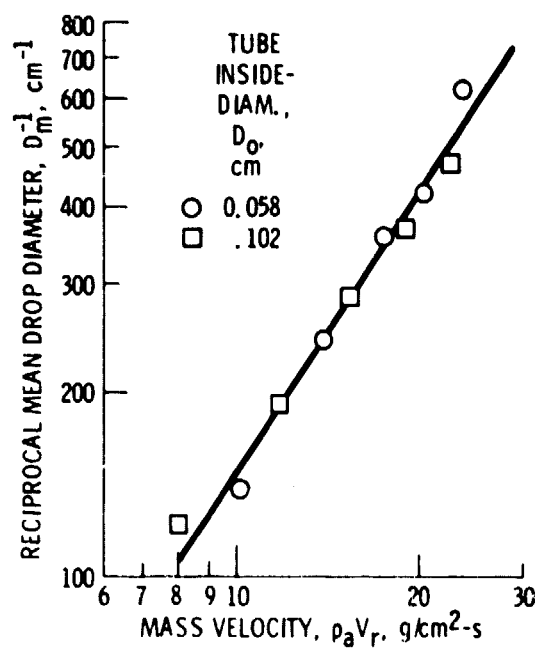


Figure 9. - Variation of reciprocal mean drop diameter with mass velocity. Axial upstream injection in axial airflow.

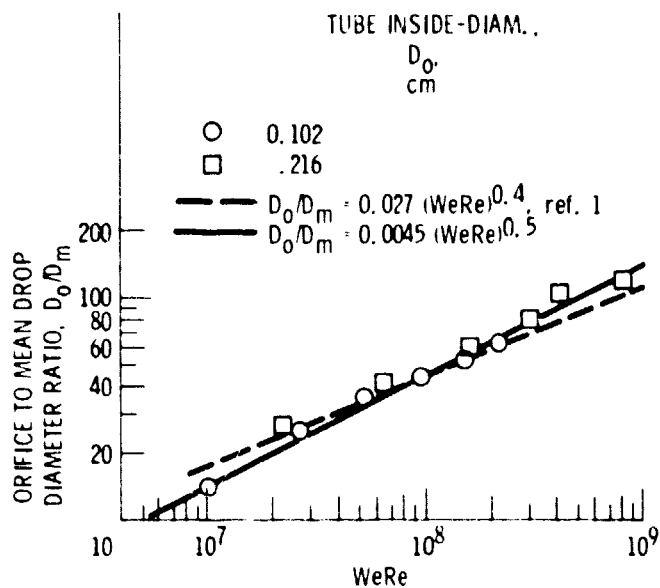


Figure 10. - Variation of orifice to mean drop diameter ratio with product of the Weber and Reynolds number. Axial upstream injection in axial airflow.